November 2004

Development of Intermediate-Temperature Solid Oxide Fuel Cells for Direct Utilization of Hydrocarbon Fuels

C. Lu
University of Pennsylvania

Sungbae An
University of Pennsylvania

Wayne L. Worrell
University of Pennsylvania

John M. Vohs
University of Pennsylvania, vohs@seas.upenn.edu

Raymond J. Gorte
University of Pennsylvania, gorte@seas.upenn.edu

Postprint version. Published in *Solid State Ionics*, Volume 175, Issues 1-4, 30 November 2004, pages 47-50.
Publisher URL: http://dx.doi.org/10.1016/j.ssi.2004.09.019

Development of Intermediate-Temperature Solid Oxide Fuel Cells for Direct Utilization of Hydrocarbon Fuels

Abstract
In this study, we compare the performance of SOFC having composite Cu-based anodes but made with the following low-temperature electrolytes: samaria-doped ceria (SDC), Sr- and Mg-doped lanthanum gallate (LSGM), and scandia-stabilized zirconia (ScSZ). Performance (V-I) curves and impedance spectra were measured using H_2 and *n*-butane fuels at 973 K. The results suggest that the use of electrolyte materials with higher ionic conductivity can lead to improved anodes for direct-utilization SOFC, although the performance of each of the cells in *n*-butane appears to be at least partially limited by the electrochemical oxidation reaction.

Keywords
Intermediate temperature, Solid oxide fuel cells, Copper-ceria anodes, n-butane

Comments
Postprint version. Published in *Solid State Ionics*, Volume 175, Issues 1-4, 30 November 2004, pages 47-50.
Publisher URL: http://dx.doi.org/10.1016/j.ssi.2004.09.019

Development of Intermediate-Temperature Solid Oxide Fuel Cells for Direct Utilization of Hydrocarbon Fuels

C. Lu[1], S. An[1], W. L. Worrell[1], J. M. Vohs[2], and R. J. Gorte[2]

Department of Materials Science and Engineering[1]

and Department of Chemical and Biomolecular Engineering[2]

University of Pennsylvania

Philadelphia, PA 19104-6272

Abstract

In this study, we compare the performance of SOFC having composite Cu-based anodes but made with the following low-temperature electrolytes: samaria doped ceria (SDC), Sr- and Mg-doped lanthanum gallate (LSGM), and scandia-stabilized zirconia (ScSZ). Performance (V-I) curves and impedance spectra were measured using H_2 and n-butane fuels at 973 K. The results suggest that the use of electrolyte materials with higher ionic conductivity can lead to improved anodes for direct-utilization SOFC, although the performance of each of the cells in n-butane appears to be at least partially limited by the electrochemical oxidation reaction.

PACS/Keywords: 84.60.Dn/Intermediate temperature, solid oxide fuel cells, copper-ceria anodes, n-butane.

Introduction

Solid oxide fuel cells (SOFCs) have the ability to provide electrical energy with high efficiency and low environmental impact (1). However, the high operating temperatures (> 1073 K) that are required for conventional SOFCs based on yttria-stabilized zirconia (YSZ) require the use of expensive materials and lead to significant problems with seals and interconnects. The development of intermediate-temperature SOFCs could extend cell lifetimes, make it possible to use inexpensive metal components as interconnects, and reduce fabrication costs. Among alternative electrolyte materials, several of the most promising are samaria doped ceria (SDC), Sr- and Mg-doped lanthanum gallate (LSGM), and scandia-stabilized zirconia (ScSZ). High performance SOFCs have been prepared with each of these electrolytes using Ni-based anodes and H_2 as the fuel (2-7).

However, Ni-based anodes have severe fuel limitations, especially at lower temperatures. First, the equilibrium constant for steam reforming is unfavorable at temperatures below ~973 K, requiring higher steam contents in the feed. Even more significant, Ni catalyzes the formation of carbon fibers when exposed to dry hydrocarbons, causing rapid deactivation. The formation of Ni carbides can even cause the cell to fracture. Obviously, there would be advantages to replacing Ni with a material that would be stable in the presence of a wide range of fuels. Ideally, the ability to use hydrocarbons directly, without reforming, could greatly simplify the overall fuel-cell system.

It has recently been demonstrated that it is possible to directly utilize a wide variety of hydrocarbon fuels, including liquids such as diesel (8,9), when Ni is replaced

with Cu in the SOFC anode. Cu is a poor catalyst for making and breaking C-C bonds, so that it does not promote graphite formation. It appears that Cu serves primarily as an electronic conductor in the anodes and that an additional oxidation catalyst must be added in order to achieve reasonable performance (10). In most of the work from our laboratory, that oxidation catalyst has been ceria (8,11), so that the anode for a YSZ electrolyte is a composite of Cu (for electronic conductivity), ceria (for oxidation activity and possibly mixed conductivity), and YSZ (for ionic conductivity).

Although the direct utilization of hydrocarbons has been demonstrated in Cu-ceria-YSZ anodes, only a limited amount of work has been performed with alternative electrolytes that could allow for operation at lower temperatures (12). In the present study we have extended previous investigations with SDC electrolytes to ScSZ and LSGM electrolytes. As in past work, the anode was again a composite of Cu, ceria, and the electrolyte. The performance and electrochemical characteristics of these cells while operating on both H_2 and C_4H_{10} fuels at 973 K are reported.

Experimental

The ScSZ (9mol%Sc_2O_3) powder was prepared using a co-precipitation technique (12), while the LSGM ($La_{0.8}Sr_{0.2}Ga_{0.8}Mg_{0.2}O_{3-\delta}$, Praxair^{TM}) and SDC ($Sm_{0.2}Ce_{0.8}O_{1..9}$, Praxair^{TM}) were used as received. The initial step in the fabrication of all the cells involved making a bilayer (one side porous and the other dense) of the electrolyte material. After attaching the cathode material to the dense side of the wafer, ceria and Cu were added to the porous side by wet impregnation with soluble salts to achieve the desired final compositions. (Note: As shown elsewhere, it was important to add ceria

even to the cell based on SDC (11). Cells made without ceria performed very poorly, especially with n-butane.)

For SDC and LSGM, the bilayer was prepared by simply pressing powders of the electrolyte materials (11). Some of the SDC or LSGM powder was mixed with controlled amounts of graphite pore formers in acetone and pressed; then, a layer of the pure SDC or LSGM powder was distributed over the initial wafer and pressed again to form a green body. This green body was heated in air to 1673 K for SDC and 1723 K for LSGM. For the ScSZ cells, the bilayer was produced using a dual tape-casting method, with one tape containing graphite and polymethyl methacrylate (PMMA) pore formers, that has been described elsewhere (12). The tapes were calcined at 1723 K for 4 h. Microstructures of the cells were observed using a JEOL6400 scanning electron microscope (SEM). The cell dimensions, determined from the SEM micrographs, are listed in Table 1.

For the cathodes on the SDC and LSGM cells, a 50 wt-% mixture of the electrolyte powder and lanthanum strontium cobalt ferrite (LSCF, Nextech^{TM}) was pasted onto the exposed surface of the dense membrane with glycerol and fired in air at 1273 K for 1 h. For the ScSZ cell, a similar approach was used to attach the LSM ($La_{0.8}Sr_{0.2}MnO_3$)-ScSZ (50 wt%) composite cathode, except the calcination conditions were 1523 K for 2 h. The cell anodes were prepared by wet impregnation with aqueous solutions of $Ce(NO_3)_3$ and $Cu(NO_3)_2$, with the Ce and Cu solutions added in separate steps, with calcination to 723 K to decompose the nitrates after each step. The copper oxide was reduced to Cu metal in flowing H_2 during the initial heating of the fuel cell for testing. The final anode compositions for each of the cells that were tested are summarized in Table 1.

For electrical connections, we used a Pt mesh and Pt paste (Engelhard, A4338) for the cathode and a Au mesh with Au ink (Engelhard, A3360) for the anode. The single cells were then attached to an alumina-support tube using a high-temperature ceramic cement (Aremco; Ceramabond 571).

Dry H_2 and C_4H_{10} were fed to the anode at a flow rate of 20 ml/min, while the cathode was exposed to air. Both the performance (I-V) curves and impedance spectra were measured using a computer-controlled Solartron 1287 electrochemical interface and a Solartron 1250 frequency response analyzer. Impedance spectra were carried out in a frequency domain from 0.01 Hz to 65 kHz over a range of current densities, starting from the open-circuit voltage (OCV), although the measurements reported here were all obtained at a current density of 0.2 A/cm^2.

Results and Discussion

The performance curves in H_2 and n-butane at 973 K for cells made from all three electrolyte materials are shown in Figs 1 and 2 respectively. With H_2, the OCV for the cells based on LSGM and ScSZ were close to 1.2 V, indicating that there were no significant leaks in the electrolyte or seals. However, for the SDC-based cell, the OCV was only ~0.85 V, probably due to mixed conductivity of the SDC under reducing conditions, a problem that is not observed with the LSGM or ScSZ, which are almost pure ionic conductors in the fuel cell environment (3,7). At 700^{o}C cell maximum power densities with H_2 fuel are 0.30 W/cm^2, 0.22 W/cm^2 and 0.29 W/cm^2 for the cells based on SDC, LSGM, and ScSZ, respectively.

It must be noted that the data in Fig. 1 were taken after conditioning each of the cells in dry n-butane for 20 min. For the SDC-based cell, this conditioning had no effect on the V-I curves; however, this conditioning resulted in a significant increase in the performance curves for the cells based on ScSZ and LSGM. As discussed in a recent paper on YSZ-based cells (13), exposure of the anode to dry hydrocarbons results in the deposition of tar that enhances the electronic conductivity in the anode when there is insufficient Cu. In the case of the SDC cell, this enhanced conductivity may not be necessary due to the electronic conductivity of the SDC itself under reducing conditions. In the case of the cells based on LSGM and ScSZ, this enhancement was crucial for obtaining high performance with relatively low Cu contents.

Each of the three cells with the Cu-ceria based anodes showed stable performance in dry n-butane at 973 K, and the V-I performance curves for this fuel are shown in Fig. 2. Again, higher OCVs were observed with the cells based on LSGM and ScSZ than were observed with SDC cell due to mixed conductivity of the SDC. Given that the Nernst potential for n-butane at standard conditions should be 1.1 V, even the potentials for the LSGM and ScSZ cells are low. As suggested elsewhere, the low potential is probably due to the complexity of the reaction (26 electrons), which likely requires multiple steps, allowing equilibrium to be established with surface intermediates other than CO_2 and water (8). The maximum power densities for the cells based on SDC and ScSZ were surprisingly similar, 0.18 and 0.15 W/cm^2, respectively. It is interesting to notice that this is also very similar to the power densities observed with the related, YSZ-based cells (13). The maximum power density for the LSGM cell was significantly lower, approximately 0.09 W/cm^2.

To gain insights into the factors that limit performance in these three cells, the impedance spectra in Figs. 3 and 4 were measured. Fig. 3 shows Cole-Cole Plots of the cells based on SDC, LSGM, and ScSZ in H_2 at 973 K, at a current density of 0.2 A/cm^2. The ohmic resistances, R_r, measured from the high-frequency intercepts with the real axis, are due primarily to contributions from the electrolyte. The total cell resistances, R_t, are determined from the low-frequency intercept and should be equal to the slope of the V-I curves at the current density of the measurement. For the three cells that were studied, R_r and R_t were 0.44 and 0.55 $\Omega \cdot cm^2$ for the SDC cell, 0.88 and 1.4 $\Omega \cdot cm^2$ for the LSGM cell, and 0.44 and 1.3 $\Omega \cdot cm^2$ for the ScSZ cell.

These values for R_r and R_t lead to several interesting implications. First, while the R_r for the SDC and ScSZ cells are perhaps slightly higher than one would expect based on the conductivities of these materials and the thickness of the electrolytes, the ohmic resistance of the LSGM cell is much higher than would be expected, suggesting that some of the ohmic resistance must be from the electrodes. This is probably due to the low porosity of the LSGM anode and the small amount of Cu that could be added to this cell. Second, the impedance due to the electrodes is significantly smaller on the SDC cell than on the LSGM or ScSZ cells. This is probably due to the expanded three-phase boundaries resulting from the mixed-conductivity of the SDC.

The analogous results for the three cells in n-butane are shown in Fig. 4, again at a current density of 0.2 A/cm^2. As expected, the ohmic resistances determined from these impedance spectra are essentially the same as those determined using H_2 as the fuel. The major change comes in the size of the non-ohmic component associated with the electrodes. The total cell resistances in n-butane were 1.05 $\Omega \cdot cm^2$ for the SDC cell, 2.0

$\Omega \cdot cm^2$ for the LSGM cell, and 1.4 $\Omega \cdot cm^2$ for the ScSZ cell. While the increase in R_t over that observed in H_2 was small for the ScSZ cell, probably due to artifacts associated with the highly nonlinear shape of the V-I curve, the total resistance of the SDC and LSGM cells increased by 0.6 $\Omega \cdot cm^2$. While changes in electrolyte thickness and improvements in the microstructure of the electrodes is likely to decrease the overall cell impedances, this resistance is likely associated with activation of the hydrocarbon fuel. Lowering this value will require improvements in the catalytic properties of the anode.

When these results are compared to published data on similar YSZ-based cells (13), it appears that the electrode resistances in n-butane are lower, at least in the SDC and LSGM cells. Since each of the cells had a similar pore structure and each had similar Cu and ceria contents, we suggest that differences between the YSZ-based cells and the SDC- and LSGM-based cells may be due to increased mobility of oxygen ions within the electrolyte matrix in the anodes. There is internal evidence for this in the impedance spectra. The increased resistance in going from H_2 to n-butane in each of the cells is clearly associated with low-frequency arcs in the impedance spectra. Low-frequency processes are almost certainly due to diffusion, probably of oxygen ions within the electrolyte matrix in the anode. Given that these frequencies are quite different for the various electrolyte materials, one should expect the composition and structure of the electrolyte to affect performance.

The results in this paper suggest that significant improvements in anode performance can be achieved through the use of alternative electrolyte materials with the anodes of direct-utilization SOFC. We are presently working to identify the experimental factors that can provide these improvements.

Summary

Alternative electrolyte materials show great promise for use in the anodes of SOFC that directly utilize hydrocarbon fuels. The improved ionic conductivity appears to improve anode performance through improved ionic conductivity within the anode. However, to utilize this intrinsic advantage, it is necessary to obtain the proper microstructure within the anode material.

Acknowledgement

This work was supported by the Army Research Laboratory-Collaborative Technology Alliance (ARL-CTA) in Power and Energy.

References

1. N. Q. Minh and T. Takahashi, *Science and Technology of Ceramic Fuel Cells*, Elsevier 1995.

2. C. Xia, F. Chen and M. Liu, *Electrochemical and Solid-State Letters*, **4** (5) A52-A54 (2001).

3. K. Huang, R. Tichy and J. Goodenough, *J. Am. Ceram. Soc.,* **81** (10), 2581-85 (1998).

4. X. Zhang, S. Ohara et al, *J. Power Source,* **83** (1999)170-177.

5. R. Doshi, V. Richards, J. D. Carter, X. Wang, and M. Krumpelt, *J. Electrochem. Soc*., **146** (4), 1273-1278 (1999).

6. M. Mogensen, N. Sammes and G. Tompsett, *Solid State Ionics*, **129** , 63-94 (2000).

7. S.P.S. Badwal, F.T. Ciacchi and D. Milosevic, *Solid State Ionics*, **136 -137** 91 (2000).

8. S. Park, J. Vohs, and R. Gorte, *Nature*, **404**, 265 (2000).

9. H. Kim, S. Park, J. Vohs and R. Gorte, *J. Electrochem. Soc.,* **148** (7), A693 (2001).

10. C. Lu, W. L. Worrell, J. M. Vohs and R. J. Gorte, *in Solid Oxide Fuel Cells VIII,* The Electrochemical Society, Pennington, NJ (2003), in press.

11. C. Lu, W. L. Worrell, J. M. Vohs and R. J. Gorte, *J. Electrochem. Soc.,* **150** (3), A354-A358 (2003).

12. S. An, C. Lu, W. L. Worrell, J. M. Vohs, and R. J. Gorte, in *Solid-State Ionics Devices III*, The Electrochemical Society Proceeding Series, in pressed.

13. S. McIntosh, J. M. Vohs, and R. J. Gorte, *J. Electrochem. Soc.*, **150** (4), A470-A476 (2003).

Table 1. Properties of cells used in this study.

Cell	Electrolyte		Anode			
	Type	Thickness (μm)	Composition		Porosity (vol%)	Thickness (μm)
			Cu (wt%)	Ceria (wt%)		
1	SDC	~ 340	36	16	55	~ 150
2	LSGM	~ 440	10	10	35	~ 330
3	ScSZ	~ 60	20	20	60	~ 300

Figure Captions

Figure 1. Cell potentials and power densities as a function of current density with H_2 fuel at 700^{o}C for the SDC cell (□); the LSGM cell (○); and the ScSZ cell (Δ).

Figure 2. Cell potentials and power densities as a function of current density with C_4H_{10} fuel at 700^{o}C for the SDC cell (□); the LSGM cell (○); and the ScSZ cell (Δ).

Figure 3. Impedance spectra with H_2 fuel at 700^{o}C for the SDC cell (□); the LSGM cell (○); and the ScSZ cell (Δ). (measured under constant current 0.2 A/cm^2)

Figure 4. Impedance spectra with C_4H_{10} fuel at 700^{o}C for the SDC cell (□); the LSGM cell (○); and the ScSZ cell (Δ). (measured under constant current 0.2 A/cm^2)

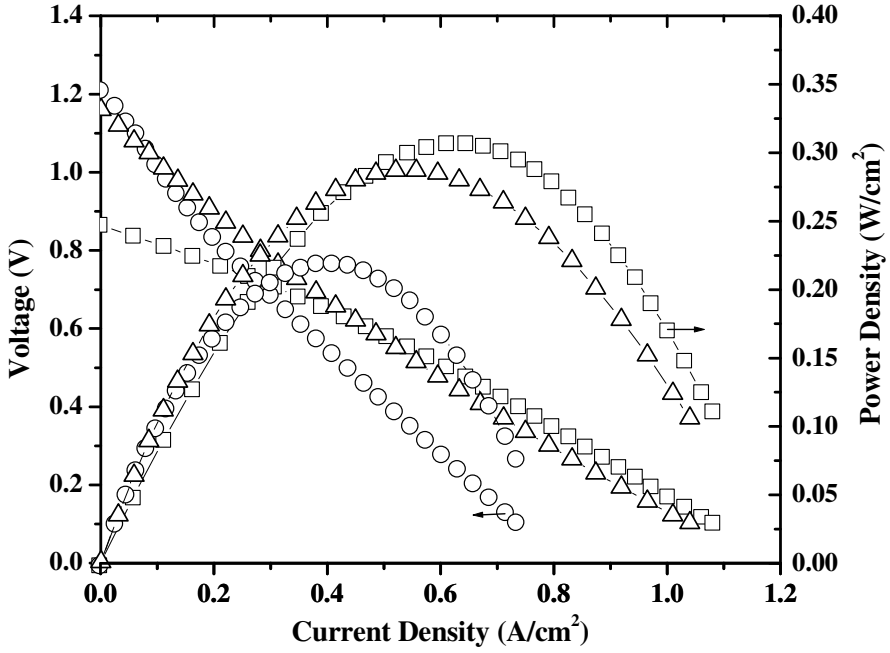
Voltage (V)
Power Density (W/cm^2)
Current Density (A/cm^2)
1.4
1.2
1.0
0.8
0.6
0.4
0.2
0.0
0.40
0.35
0.30
0.25
0.20
0.15
0.10
0.05
0.00
0.0
0.2
0.4
0.6
0.8
1.0
1.2

Fig 1.

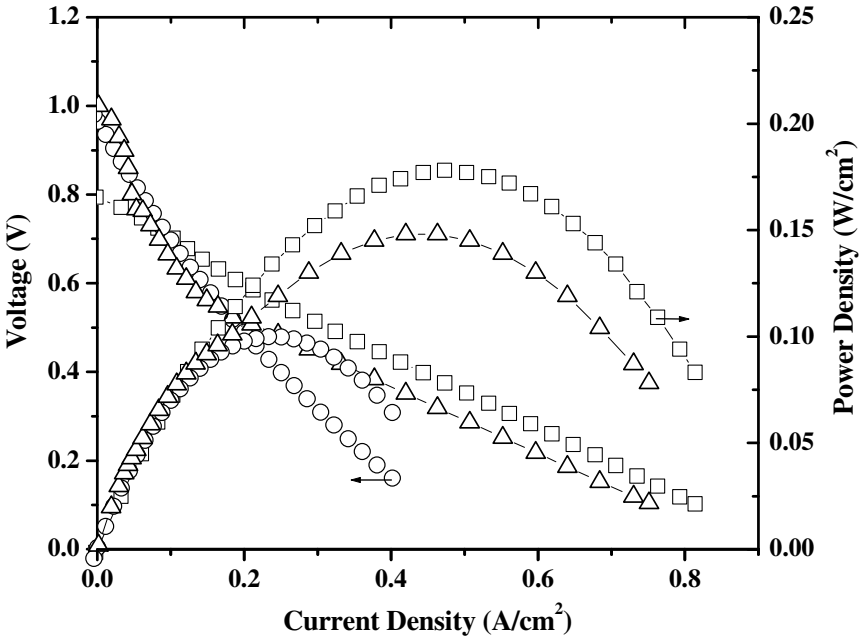
Voltage (V)
Power Density (W/cm^2)
Current Density (A/cm^2)
1.2
1.0
0.8
0.6
0.4
0.2
0.0
0.25
0.20
0.15
0.10
0.05
0.00
0.0
0.2
0.4
0.6
0.8

Fig. 2

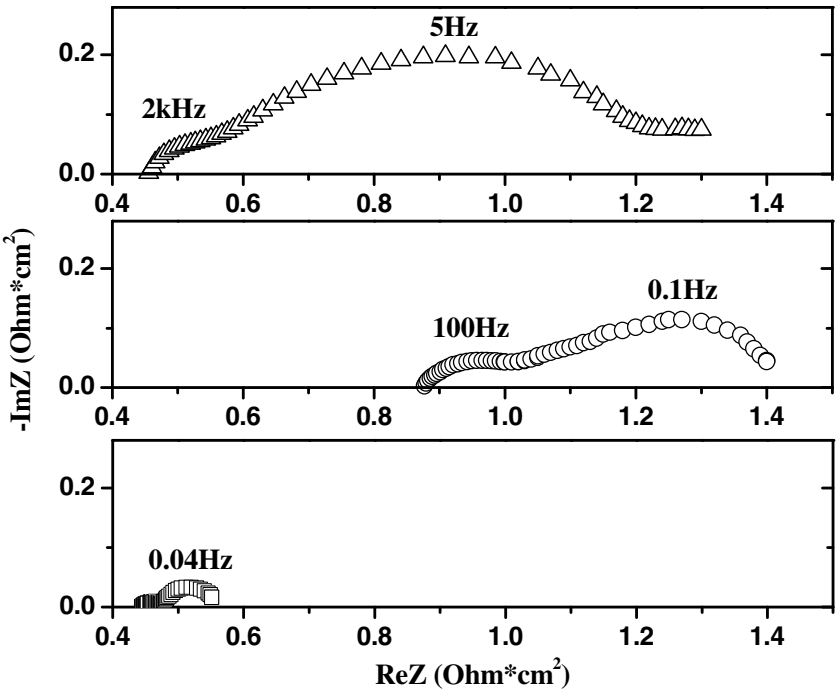
5Hz
2kHz
0.1Hz
100Hz
0.04Hz
0.0
0.2
0.4
0.6
0.8
1.0
1.2
1.4
-ImZ (Ohm*cm2)
ReZ (Ohm*cm2)

Fig. 3

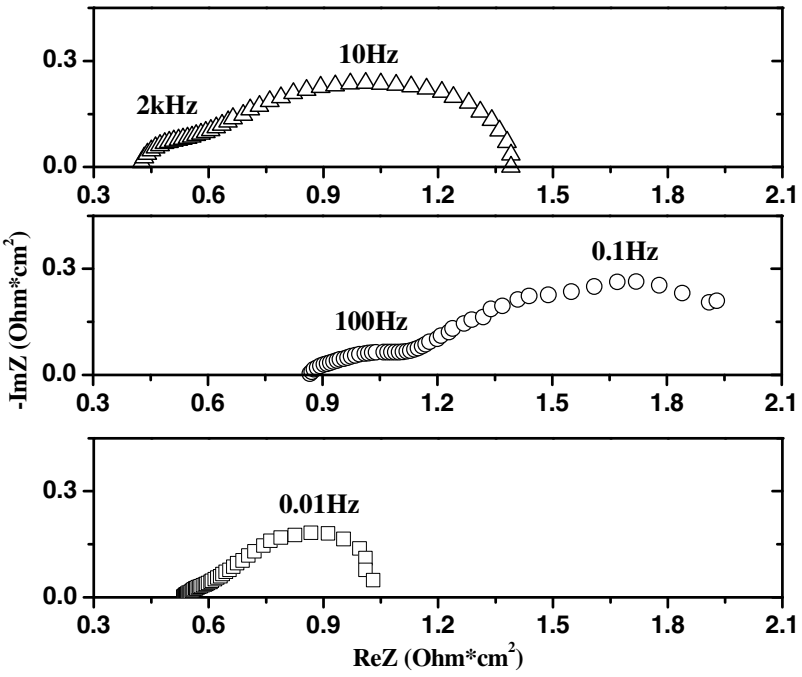
10Hz
2kHz
0.1Hz
100Hz
0.01Hz
-ImZ (Ohm*cm^2)
ReZ (Ohm*cm^2)
0.0
0.3
0.6
0.9
1.2
1.5
1.8
2.1

Fig. 4